

Evolution of Thermal and Mechanical Properties of Mine Tailings and Fly Ash Mixtures during Curing Period

Joon Kyu Lee and Julie Q. Shang

The University of Western Ontario
Department of Civil and Environmental Engineering Faculty of Engineering Science



Evolution of Thermal and Mechanical Properties of Mine Tailings and Fly Ash Mixtures during Curing Period

Joon Kyu Lee¹ and Julie Q. Shang²

Abstract: Fly ash is often used as a binder for modifying the properties of geomaterials such as organic and expansive soils, sludge from water treatment, dredged sediments, mine tailings, etc. In this study, the thermal and mechanical properties of compacted mixtures of mine tailings and fly ash are studied over the curing period of 120 hours. The study includes through the measurement of thermal conductivity, temperature, unconfined compressive strength and elastic modulus. The effects of the amount of fly ash added to mine tailings, molding water content and compaction energy on these properties are investigated. The pore size distribution and surface texture are analyzed to characterize the microfabrics of fly ash treated mine tailings. Relationships between the thermal conductivity and properties that capture packing and mechanical characteristics of mine tailings and fly ash mixtures are established. These observations provide enhanced understanding of heat transport through geomaterials with fly ash as an additive, which will be beneficial for quality control and assurance in related engineering applications.

Key words: Thermal conductivity; Temperature; Unconfined compressive Strength; Elastic modulus; Mine tailings; Coal fly ash

¹PhD Candidate, Dept. of Civil and Environmental Engineering, Univ. of Western Ontario, London, ON, Canada N6A 5B9 (Corresponding author). E-mail: jlee962@uwo.ca

²Professor, Dept. of Civil and Environmental Engineering, Univ. of Western Ontario, London, ON, Canada N6A 5B9. E-mail: jqshang@uwo.ca

Introduction

Fly ash is a by-product of the combustion process in coal-fired power generating plants, which mostly consists of smooth spherical particles of silicon, alumina, iron and calcium oxides, along with residual carbon. Coal fly ash is commonly used alone or as an admixture in construction owing to its pozzolanic, cementitious and alkaline nature. The classification and characterizing method of fly ash for use in civil engineering applications are reviewed in ASTM C618 (ASTM 2008a) and ASTM D5239 (ASTM 2004). When fly ash is added to a soil-water system, lime (CaO), the reactive component, reacts with water and soil solids, resulting in cation exchange, flocculation, carbonation and pozzolanic reactions. These reactions lead to significant changes in the geochemical and mineralogical properties and the microfabric of the geomaterial (Choquette et al. 1987; Al-Rawas 2002; Peethamparan et al. 2008; Horpibulsuk et al. 2009). The variations in the physicochemical properties of the fly ash also cause changes to the thermal and mechanical properties of the geomaterial. Since thermal conductivity is related to the structure of geomaterials, including the size, shape, gradation and aggregation of particles, and binding agents that can be of natural and/or artificial origins (Cote and Konrad 2009), it is often used to assess the thermal properties of geomaterials. Also, as hydration of lime usually accompanies exothermic reactions, the fly ash added to a particular geomaterial induces temperature variations during the process. On the other hand, the addition of fly ash into geomaterials can often improve their engineering properties, such as strength and stiffness. These potential enhancements result from the formation of cementitious compounds such as calcium silicate hydrate (CSH) and calcium aluminate hydrate (CAH). The effectiveness of fly ash as a binder to stabilize geomaterials has been studied by examining compaction and compressibility characteristics (Nalbantoglu and Tuncer 2001), swelling (Phanikumar and Sharma 2007), California bearing ratio (Edil et al. 2006), unconfined compressive strength (Tastan et al. 2011) as well as elastic

and resilient moduli (Solanki et al. 2009). Even though numerous studies have been carried out to explore the role of fly ash as a geomaterial amendment, most works have highlighted effects on the mechanical performance in particular. In contrast, the effects of fly ash on thermal properties change have not been reported in the literature and the relationship of the thermal conductivity with the strength gain for fly ash treated geomaterials is not fully understood.

The global mining industry generates massive residue or tailings after extracting valuable metals and minerals from ore. The management and disposal of tailings pose major challenges to efforts to protect the environment. Typically, mine tailings are stored on site in the form of impoundments. In order to improve disposal efficiency, new and modified tailings management approaches have been studied and implemented: these include densification, desulphurization, and co-disposal of tailings and waste rock (Bussiere 2007). To control and mitigate the impact of acid mine drainage (AMD), several researchers (Wang et al. 2006; Yeheyis et al. 2009) have assessed the feasibility of utilizing fly ash in tailings management. It has been shown that the pozzolan stabilized tailings exhibit resistance to AMD generation and migration because of two factors, namely, the neutralization effect of the coal fly ash and formation of hydration products that act as oxygen and infiltration barriers. Mine tailings have been used in geoenvironmental applications, for instance, cemented tailings backfill (Helinski et al. 2011), engineering barrier of bentonite-tailings mixtures (Fall et al. 2009) and tailings-based pavement subbase (Qian et al. 2011). Mine tailings can be employed as fill materials if the potential of AMD generation is prohibited by adding binders such as cement, lime and fly ash where natural soils are not available in abundant quantity. In addition, knowledge of both the thermal and mechanical properties of fill materials with binders added is important for thermo-mechanical analyses of

underground structures such as oil and gas pipelines, electric transmission lines, energy piles and nuclear waste repositories.

This study is concerned with the beneficial use of mine tailings for fills with fly ash as a binder. A series of laboratory tests were conducted on compacted mixtures of mine tailings and coal fly ash obtained from a mine site and a power generating station, respectively, both in Ontario, Canada. The test specimens were prepared by controlling the amount of fly ash added to mine tailings, molding water content and compaction energy. Changes in thermal conductivity, temperature, unconfined compressive strength and elastic modulus of the specimens were monitored during the curing period. The microfabrics of the specimens were examined in terms of pore size distribution and particle surface characteristics. The relationships between thermal conductivity and the bulk unit weight and unit pore volume were established. Additionally, the correlation between thermal conductivity and the compressive strength of the specimens was observed.

Materials

In this study, mine tailings, fly ash and water were the host materials used to make the compacted mixtures of mine tailings and fly ash. The physical properties and oxide composition of mine tailings and fly ash are summarized in Tables 1 and 2, respectively. The particle size distributions of both the mine tailings and fly ash are shown in Fig. 1.

Mine Tailings

The mine tailings were taken in a dry state from the Musselwhite gold mine located in northern Ontario, Canada. The specific gravity of the tailings is 3.37, which is greater than that of most soils due to predominant amphibole minerals with high specific gravity. The tailings are

primarily comprised of silt-sized particles (83.2%) with some sand-sized (9.4%) and clay-sized (7.4%) particles. According to the Unified Soil Classification System, the tailings are classified as silts of no plasticity (ML), similar to most of the tailings produced in Canadian hard rock mines (Bussiere 2007). Meanwhile, the major oxides in the tailings include silica (50.82%), alumina (8.87%) and ferric oxide (28.97%), which account for a total amount of 88.66% by weight (Wang et al. 2006). The calcium oxide is relatively low at 3.19%.

Fly Ash

The coal fly ash was collected in a dry state from the Atikokan Thermal Generating Station located in Ontario, Canada. The specific gravity of the fly ash is 2.54, and it does not exhibit any plasticity. The fly ash is made up 98.7% fines ($< 75 \mu\text{m}$) with predominately silt-sized particles. The major oxides identified include silica (37.99%), alumina (19.92%) and ferric oxide (6.17%), with a total of 64.08% by weight (Wang et al. 2006). Thus, the Atikokan fly ash is classified as neither Class C nor Class F fly ash in accordance with ASTM C618 (ASTM 2008a). The fly ash has a high content of calcium oxide (15.66%), which is the source of pozzolan. The ratios of CaO/SiO_2 and $\text{CaO}/(\text{SiO}_2 + \text{Al}_2\text{O}_3)$, which are indicators of cementing potential (Cetin et al. 2010; Tastan et al. 2011), are calculated to be 0.41 and 0.27, respectively.

Water

Deionized water with a temperature of $22.5 \pm 0.2 \text{ }^\circ\text{C}$ was used in this study. The deionized water has a pH of 6 and electrical conductivity below $1 \mu\text{S}/\text{m}$.

Specimen Preparation and Testing Conditions

The fly ash ratio R_{FA} is based on the dry weight of solid minerals and defined as

$$[1] \quad R_{FA} = \frac{W_{FA}}{W_{MT}} \times 100 (\%)$$

where W_{FA} is the weight of fly ash and W_{MT} is the weight of mine tailings. The eight slurries of mine tailings and fly ash mixtures were prepared by adding various weights of fly ash into tailings of 25 g dispersed in 100 mL deionized water. The fly ash ratios of the mixtures ranged from 0% to 60%. The slurries were shaken at a constant temperature of 25 °C. The pH of the slurry was measured using a pH meter calibrated before measurement. The pH of each slurry was measured at 1, 24, 72 and 120 hours after mixing. It was observed that the slurry pH reached equilibrium within 1 hour after mixing the mine tailings and fly ash. Figure 2 shows the pH values measured in slurries with different fly ash ratios at 1 hour after mixing. The original tailings are slightly alkaline with pH 8.35. With increasing fly ash contents in the mixtures, the pH increases until it reaches a constant when the fly ash ratio is above 20%. Based on these results, fly ash ratios of 20, 40 and 60% were selected for the mixture specimens in this study because these fly ash ratios will sustain the physicochemical reactions required to bind the tailings.

The mixtures with the fly ash ratios of 20, 40 and 60% were thoroughly mixed in a dry state. A series of standard Proctor compaction tests [ASTM D698 (ASTM 2007)] were carried out to determine the optimum water content (OWC) and maximum dry unit weight (MDW) of all mixtures that were produced by mixing 30 minutes after adding water into the dry mixtures. In this study, all mixtures were compacted at their specific OWC and MDW. Figure 3 compares the compaction results on the mixtures with fly ash ratios of 20, 40 and 60%.

In the case of mixtures with a fly ash ratio of 20%, three compaction states were considered in order to explore effects on the thermal, mechanical and microfabric characteristics of the

specimens: (1) at the water content of 0.85 OWC (representing the dry side of optimum) under standard Proctor energy (590 kJ/m^3); (2) at the water content of 1.15 OWC (representing the wet side of optimum) under standard Proctor energy; and (3) at the OWC under high Proctor energy ($1,190 \text{ kJ/m}^3$). The high Proctor compaction was implemented using the same procedure specified for standard Proctor compaction but the compacted layers were increased from 3 to 5 and the number of blows per layer was increased from 25 to 30. It is noted that the high Proctor energy applied in this study is less than the modified Proctor energy ($2,690 \text{ kJ/m}^3$) declared in ASTM D1557 (ASTM 2009a) because the thermal properties analyzer used could not be inserted to the specimen compacted under the modified Proctor energy without a pre-drilled hole. The compaction states were designed to simulate possible field conditions.

In this study, the specimens were named in three terms. The first term indicates the fly ash (FA) ratio; the second term indicates the compaction energy, i.e., standard Proctor (SP) energy or high Proctor (HP) energy; and the third term indicates the specimen under optimum water content (OWC), dry water content (DWC) or wet water content (WWC). For example, a specimen with the fly ash ratio of 20% compacted at the standard Proctor energy and optimum water content is designated as FA20-SP-OWC. A total of six specimens were tested: FA20-SP-OWC, FA40-SP-OWC, FA60-SP-OWC, FA20-SP-DWC, FA20-SP-WWC and FA20-HP-OWC. Table 3 presents the water contents and dry unit weights for all specimens studied.

Five identical samples were made under each Specimen ID. One was used to measure the thermal conductivity and temperature during the curing period as well as to study pore size distribution and surface fabric, whereas the other four were used to evaluate changes in unconfined compressive strength and elastic modulus over time. To minimize internal variability of the samples, an automatic compaction apparatus was utilized.

Experiments

The experimental program included the measurement of the thermal conductivity, temperature, compressive strength, elastic modulus, mercury intrusion porosimetry and scanning electron microscopy of compacted mixtures of mine tailings and fly ash mixtures. The experimental devices, techniques and methodology adopted in this study are described in the following sections.

Thermal Properties Analyzer

The thermal conductivity and internal temperature during the curing of compacted mine tailings and fly ash mixtures were measured by using a KD2 Pro thermal properties analyzer. The analyzer is comprised of a micro-controller and a sensor. The controller displays automatic readings of the thermal properties and allows a user to program the analyzer to periodically measure and store these properties. The sensor has a single probe of 2.4 mm diameter and 100 mm length, mounted with a heater and a thermistor. The operating principle of the measurement system is based on the transient line heat source theory, which conforms to ASTM D5334 (ASTM 2008b). A heat pulse is applied to the heater and the temperature change within the probe is simultaneously recorded by the thermistor: the higher thermal conductivity of the medium exhibits a higher rate of heat dissipation that leads to a lower rate of temperature increase detected with the thermistor. Thermal conductivity is determined by the temperature response with time. The KD2 Pro analyzer reproduces the thermal conductivity of reference materials with $\pm 5\%$ accuracy within the temperature range of $- 50\text{ }^{\circ}\text{C}$ to $150\text{ }^{\circ}\text{C}$.

After preparing the compacted specimen, comprised of mine tailings and fly ash mixtures, the single probe sensor was vertically inserted into the specimen in the mold. In order to

minimize frictional resistance between the probe and specimen, the probe was coated with a thin layer of thermal grease. Afterward, the specimen was extruded from the mold using a hydraulic jack and immediately placed in an environmental chamber at 60% relative humidity and 24.6 °C temperature for curing. The first measurements of the thermal conductivity and temperature of the specimen were carried out within 5 minutes after compaction and were continuously monitored every 30 minutes up for a period of 120 hours.

Unconfined Compression Test

To characterize the strength and stiffness of compacted mixtures of mine tailings and fly ash, unconfined compression tests were conducted according to ASTM D5102 (ASTM 2009b). Cylindrical specimens (101.6 mm diameter and 116.4 mm height) compacted in the standard Proctor mold were tested at a loading speed of 0.5 mm/min. For each specimen, four compression tests were performed on four sub-samples with identical properties, i.e., immediately after compaction, and then 24, 72 and 120 hours after compaction. The unconfined compressive strength was determined as the peak normal stress of a stress-strain curve and the corresponding elastic modulus was calculated as the slope between the origin and maximum stress, as shown in Fig. 4. It is noted that the compressive strength is influenced by the height to diameter ratio (h/d) of a specimen. Ozyildirim and Carino (2006) pointed out that the compressive strength of concrete specimens with $h/d = 1.15$ will be approximately 10% greater than that of a cylindrical specimen with the standard $h/d = 2$. In this study, the h/d ratios of all specimens for unconfined compression tests were kept constant at $h/d = 1.15$.

Mercury Intrusion Porosimetry

Mercury intrusion porosimetry (MIP) was used to quantify the pore size distribution (PSD) of the mine tailings and fly ash mixtures. The principle of the technique is that mercury, a non-wetting fluid, will not intrude the voids of a porous medium unless a sufficient pressure is applied. According to Laplace's capillarity law (known as Washburn's equation), a theoretical relation between the intrusion pressure and the pore diameter, assuming the pore is cylindrical, can be expressed as (Washburn 1921)

$$[2] \quad d_p = \frac{4T_s \cos \theta}{P}$$

where d_p is the pore diameter (μm), P is the applied intrusion pressure (MPa), T_s is the surface tension (N/m) and θ is the contact angle (degrees). As indicated in eq. [2], the pore diameter is governed by the surface tension of the mercury and the contact angle between the mercury and the pore wall. The interfacial mercury-vacuum tension at 25 °C is 0.480 N/m and the contact angle of the mercury-air interface to the solid is assumed to be equal to 140° as cited by Cuisinier et al. (2011) on lime-treated soils. The MIP device used was the Micromeritics AutoPore IV 9500 V 1.07 with a maximum intrusion pressure of 207 MPa. The MIP device measures the pore volume of mercury intruded to the medium corresponding to stepped intrusion pressures until it reaches the capacity of the system. Given the values of T_s and θ , the pore diameters intruded by mercury under each intrusion pressure is calculated by eq. [2] and the cumulative mercury volume injected versus the pore diameter of the medium can be obtained. It is noteworthy that the MIP does not provide the measurement of the true diameter of irregular pores but of the equivalent cylindrical diameter of entrance pores. The pore size distribution by the MIP is dependent on sample pretreatment, sample size and applied mercury pressure (Aligizaki 2006). Delage (2010) suggested that the freeze-drying technique appears to be the most suitable method to

avoid fabric alteration owing to shrinkage through traditional techniques such as air drying and oven drying. Penumadu and Dean (2000) recommended that the sample volume of 1,000 to 2,000 mm³ should be used for dehydration. They also revealed that for soft soil samples, the applied pressure has impact on the sample fabric, and the internal and external pressure difference in the sample at the early stage may cause changes in the inherent fabric. According to Simms and Yanful (2004), however, this effect is less important for compacted soils. Based on these considerations, the following methodology was used to remove pore water with minimum matrix deformation of compacted mine tailings and fly ash mixtures: after the completion of thermal properties measurement, a sample with the volume of about 1,000 mm³ was carefully taken from the middle of the specimen and placed immediately in liquid nitrogen. Thereafter, the frozen sample was vacuum-sublimated for 24 hours in a desiccator.

The results of a MIP test are commonly presented in terms of the cumulative pore volume per unit weight V_c versus the logarithm of the pore diameter d_p and the derivative of the cumulative pore volume V_d ($=dV_c/d(\log d_p)$) versus the logarithm of the pore diameter d_p , which are known as the cumulative intrusion curve and differential distribution curve, respectively. The larger V_d in the differential distribution curve represents the greater presence of the corresponding pore diameter in the medium.

Scanning Electron Microscopy

Scanning electron microscopy (SEM) was used for direct observation of the spatial configuration of particles in the mine tailings and fly ash mixtures, including sizes, shapes and associated pores at micro scales. The technique provides qualitative information that can be interpreted along with results of the MIP test. The sample was prepared for SEM imaging

following the same procedures as in the MIP test. The sample surface was not polished in order to preserve the macro and micro textures. The image was taken by an LEO 440 scanning electron microscope, which allows a wide range of magnification up to 1,000 times.

Results and Discussion

Compaction Characteristics

Figure 3 shows the relationship between the dry unit weight, γ_d , and molding water content, w , for compacted mine tailings and fly ash mixtures with different fly ash ratios. The maximum dry unit weights vary from 18.9 to 19.5 kN/m³, while the optimum water contents range from 11.0 to 12.4%. With the increase in the fly ash ratio the compaction curve moves downward and toward the left, indicating that MDW and OWC decrease as the fly ash ratio increases. Similar behaviors were reported for fly ash treated soils in the literature (Osinubi 1998; Degirmenci et al. 2007). The decrease in the MDW with increasing fly ash addition is attributable to the lower specific gravity of the fly ash, i.e., 2.54, as compared to 3.37 for the mine tailings. Since the mixtures become lighter, they can be advantageous for use in fill applications. It should be noted that the pore spaces of the specimens decrease as the fly ash ratio increases, which slightly compensates for the reduction of the MDW. This is explained by the packing mechanism, namely that in a mixture of particles of different sizes, the finer particles fill voids between coarser particles (Lade et al. 1998; Yilmaz 2009). On the other hand, the decrease in the OWC with the increase of the fly ash ratio is likely due to the chemical and physical reactions involving cation exchange and surface sorption as well as flocculation and agglomeration (forming flocks of particles) brought by fly ash. When the fly ash is added to mine tailings, the mixture becomes drier and more friable under the same water content owing to hydration effects:

less water will be available for the reorientation of particles in the mixture. This can be advantageous in compaction works. Furthermore, the formation of large aggregates changes the gradation of the mine tailings and fly ash mixtures, resulting in denser packing.

Thermal Conductivity

The thermal conductivity, λ , versus the logarithm of time, t , for compacted mixtures of mine tailings and fly ash are shown in Fig. 5. Generally, the thermal conductivities of the specimens decrease as curing time increases. Moreover, the initial thermal conductivity (i.e., the first measurement after compaction) and the development characteristics of thermal conductivity with time are sensitive to the fly ash ratio and compaction conditions.

Figure 5(a) illustrates the thermal conductivity of the specimens with different fly ash ratios. The initial thermal conductivities are 1.262, 1.133 and 1.074 W/mK for the fly ash ratios of 20, 40 and 60%, respectively, indicating the specimens with higher fly ash content have lower initial thermal conductivities. This is mainly attributed to the fact that the thermal conductivity of fly ash is normally lower than that of minerals in natural geomaterials (Kolay and Singh 2002). Meanwhile, as the curing time increases, the thermal conductivity difference in the specimens decreases. However, the thermal conductivities of all specimens converge at the end of the curing period. The change in the thermal conductivity within the curing time at different fly ash ratios can be explained as follows: immediately after compaction, the thermal conductivity of the specimens is affected by the thermal conductivities of their constituents; as the curing time progresses, water is consumed by evaporation and hydration. As a result, cementation develops because of cementing and pozzolanic activities in the mixtures, which generates bonding

between particles; finally, at the end of the curing period, the thermal conductivities of the specimens are governed primarily by the newly formed structure.

Figure 5(b) highlights the effect of molding water content on the thermal conductivities of the specimens with a fly ash ratio of 20%. The highest initial thermal conductivity is achieved at the optimum compaction, followed by the wet side of compaction and the dry side of compaction. At the OWC, the solid particles are in the closest arrangement, with smallest pore spaces occupied by water and air. The magnitudes of the initial thermal conductivity of the specimens compacted at the OWC, WWC and DWC can be explained by the fact that the thermal conductivity of solid minerals (1 - 10 W/mK) is much higher than that of water (0.57 W/mK) or air (0.026 W/mK). However, the significant thermal conductivity difference at different water contents disappears in the middle of the curing period (after about 5 hours) because the specimens with the same amount of fly ash result in similar levels of hydration although they have different molding water contents, as the curing time increases.

Figure 5(c) compares the thermal conductivities of two specimens with the same molding water content but different compaction energies. The higher compaction energy induces higher initial thermal conductivity, resulting from the higher density of the specimen, which means better contact between neighboring particles for heat conduction. However, the variations of thermal conductivity against curing time are relatively independent of the compaction energy.

Temperature

The internal temperature, T , of all compacted specimens of mine tailings and fly ash mixtures during curing period, t , was monitored and the results are shown in Fig. 6. The trend of the temperature fluctuation of the specimens over time is similar in all specimens: the initial

temperatures of the mine tailings and fly ash mixtures are within the range of 22 to 23 °C, which decreases in the first 5 hours of curing; then the trend is reversed, i.e., the specimen temperature increases with time until it reaches equilibrium with the environmental chamber temperature of 24.6 °C after about 90 hours. The decrease in temperature at the early curing stage for all specimens is unexpected, based on the understanding that the exothermic hydration reaction of lime (CaO) provokes the release of heat energy. One of the possible reasons for this is that the hydration of specimens releases less heat compared to the endothermic thermal energy consumed by water evaporation. This is consistent with the observation that temperature increase is related to the fly ash ratio: the higher the fly ash ratio, the higher temperature of the specimens up to a curing time of 50 hours (Fig. 6(a)). It should be also noted that the temperature change is less influenced by the molding water content and compaction energy as seen in Fig. 6(b).

Unconfined Compressive Strength

Figure 7 shows the unconfined compressive strength, q_u , of the specimens under various fly ash ratios, molding water contents and compaction energies. Figure 7(a) plots the effect of fly ash ratio on the compressive strength of mine tailings and fly ash mixtures compacted under their optimum water contents. It is observed that the compressive strength of the specimens increases as the fly ash ratio increases. For instance, after 120 hours curing, the compressive strengths of the specimens with fly ash ratios of 20, 40 and 60% are 121, 178, and 293% higher, respectively, compared with the compressive strength (0.2 MPa) of untreated mine tailings. The incidence of higher compressive strength with increasing fly ash ratio is a result of denser packing as well as cementation owing to pozzolanic reactions. On the other hand, it is found that the rate of compressive strength gain depends on the fly ash ratio: the compressive strengths of specimens with the fly ash ratios of 20 and 40% increase rapidly in 24 hours and then approach equilibrium

with further increase in curing time, whereas the compressive strengths for specimens with 60% fly ash ratio increase progressively over a period of 120 hours, as seen in Fig. 7(a). This indicates that higher fly ash content requires a longer period of curing time for the development of full strength. This result is consistent with the results of fly ash treated soils reported in the literature (Indraratna et al. 1999; Koliass et al. 2005; Ghosh and Subbarao 2007).

Figure 7(b) presents the unconfined compressive strength of the specimens with a constant fly ash ratio of 20% as influenced by the molding water content and compaction energy. The results show a similar trend of compressive strength gain against curing time. Meanwhile, the compressive strengths of the specimens compacted at the DWC are higher than that of the specimens at the OWC and WWC. It is also noted that despite the higher dry unit weight of the specimen compacted at the OWC as compared to that compacted at the DWC, the compressive strength of the former is lower than that of the latter. This is because the strength of compacted geomaterials is affected not only by the dry unit weight and water content, but also by matric suction. Many researchers (Daniel and Benson 1990; Daniel and Wu 1993; Yang et al. 2005; Guney et al. 2006; Sawangsuriya et al. 2008) have observed that higher suction leads to higher soil strength and stiffness. In addition, the strength difference that is attributable to varying water contents results in the difference in microfabrics formed during compaction. For example, Thom et al. (2007) studied the impacts of water content variation on the fabric of a compacted clayey soil. They reported a progressive growth of smaller pores linked to larger pores attenuation with the increase in the compaction water content. Therefore, the differences in the strength characteristics of the specimens are the combination of varying water content and structural differences. On the other hand, for the specimens obtained with the same molding water but different compaction energies, higher compressive strength is observed at higher compaction

energy (Fig. 6(b)), as expected. The compressive strengths of specimens compacted under high Proctor energy are 27% to 38% higher than those compacted using standard Proctor energy in all four curing periods.

Elastic Modulus

Figure 8 shows the development of the elastic modulus, E , of specimens during curing as related to the fly ash ratio, molding water content and compaction energy. It is seen that the development of elastic modulus is similar to that of the unconfined compressive strength presented in Fig. 7. In the case of the specimen compacted at the WWC, however, the increase of the elastic modulus with time is slower than the specimens molded at the OWC and DWC. This is most likely due to the fact that the WWC compacted specimens contain more water during the curing period, which lubricates interparticle contacts and facilitates the rolling and sliding of particles. As a result, the specimen can sustain larger deformation before failure.

Pore Size Distribution

Figure 9 shows the effect of fly ash ratio on the pore size distribution of compacted mixtures of mine tailings and fly ash. In Fig. 9(a), the cumulative intrusion curves are well-graded with smooth boundaries, indicating that all pore sizes lie within the detectable range. More importantly, the cumulative pore volume decreases with increasing fly ash ratio. This is attributed to the higher unit weight as a result of better packing, as noted previously. The differential pore volume distribution curves of the specimens with the fly ash ratio are illustrated in Fig. 9(b). In the case of the fly ash ratio of 20%, the PSD exhibits a bimodal feature, namely a peak at the pore diameter of 4.083 μm and another at 1.563 μm . The apparent diameter boundary between the two predominant pore diameters is 2.948 μm . Consequently, this specimen can be

characterized as having a double porosity fabric that contains significant families of both micropores and macropores. Such a microporosity fabric can be also found in other graded soils, such as compacted mixtures of sand and clay (Juang and Holtz 1985) and compacted clayey till (Simms and Yanful 2001). From the MIP results, it is believed that the characteristics of a double porosity fabric are associated with the size, shape and gradation of particles. The specimen with the fly ash ratio of 40% also displays bimodal pore distribution, but the two distinct pore diameters slightly decreases with the increase in the corresponding peak intensity when compared with the specimen with the 20% fly ash ratio. Finally, the differential distribution curve of the specimen with the fly ash ratio of 60% in Fig. 9(b) shows a smooth unimodal distribution with a dominant pore diameter of 0.984 μm . The difference between the differential distribution curves of the specimens with the fly ash ratio is explained by the packing theory of a binary mixture: when a small amount of finer particles is added to coarser particles, the mixture will have dual porosity fabric; and with increasing proportion of finer particle in the specimen, the “tightest” packing is attained, in which the fine particles more fully occupy the pores between coarser particles, resulting in a single porosity matrix. Further discussion can be made by defining a fly ash proportion, i.e.,

$$[3] \quad P_{FA} = \frac{W_{FA}}{W_{FA} + W_{MT}}$$

where parameters have been stated in eq. [1]. The results of this study show that the densest packing of compacted mine tailings and fly ash mixtures is obtained at the fly ash proportion in the mixture, P_{FA} , of 37.5%, which is corresponding to the fly ash ratio, $R_{FA} = 60\%$. The results are consistent with previous studies on porosity behaviors of binary mixtures (Piloto and Martin 2001; Thevanayagam et al. 2002; Yilmaz 2009), which found that the minimum voids of a finer

and coarser particles mixtures are achieved at a proportion of finer particles ranging between 30% and 40%.

Figure 10 highlights the influence of molding water content on the PSD of the specimens with the fly ash ratio of 20%. The lowest cumulative pore volume at a given pore diameter of 3.6 nm is obtained at the OWC, followed by the DWC and WWC, as seen in Fig. 10(a). This is in consistent with the relative order of magnitude of the corresponding dry unit weights presented in Fig. 3. Meanwhile, the differential distribution curves of all three specimens are bimodal with noticeable differences in the macropore mode, as shown in Fig. 10(b). The families of macropores shift toward the left as the water content increases from the DWC to OWC, indicating a reduction in the mean size of the macropores as the water content increases. However, there is a minor difference between the specimens compacted at the OWC and WWC. As seen in Fig. 10(b), the peak intensity of the specimen compacted at the DWC is approximately two times higher than those compacted at the OWC and WWC. In other words, the micropores remain essentially unchanged and the macropores vary correspondingly with the molding water contents. This result supports the idea that the difference in the unconfined compressive strength of the specimens with different molding water contents of mine tailings and fly ash mixtures is partially related to the difference in the microfabrics formed during the compaction process. In fact, according to Delage et al. (1996), the soil compacted on the dry side of optimum leads to aggregate-dominated fabric while the soil compacted on the optimum and the wet side of optimum creates the matrix-dominated fabric without apparent aggregates.

Figure 10 also shows comparison of the pore size characteristics of two specimens with the same fly ash ratio (20%) under different compaction energies. At a given water content, the higher compaction energy generates a specimen of lower cumulative pore volume with closely

packing (Fig. 10(a)). As seen in Fig. 10(b), the increase in the compaction energy has an effect on both macropores and micropores, although the influence on the former is more pronounced. It is also observed that the specimen compacted under high Proctor energy has a weak bimodal distribution.

SEM Image

Figure 11 shows the SEM images of compacted specimens of mine tailings and fly ash mixtures with different fly ash ratios (20, 40 and 60%) at 150 times magnification. Glassy spherical fly ash particles are coated and embedded in a tailings matrix of irregular bulky tailings minerals, which can be characterized as mine tailings-dominated fabric. It is visible in these images that two particles with different shapes are closely packed and bonded with particle-to-particle contact. More detailed observation reveals that matrices of particles in the specimens with the fly ash ratios of 20 and 40% have a more irregular prominence in the form of particle assemblages and more diversified pore sizes and larger pores in their fabrics. On the other hand, the specimen with the fly ash ratio of 60% appears to be homogeneous with a uniform distribution of pores. This observation is generally consistent with the results of pore size distributions discussed above, although a distinct bimodal porosity feature is not observed. Interestingly, most pores diameters appear to be smaller than 100 μm , which seems in agreement with the MIP results showing in Figs. 9 and 10. This can corroborate the fact that in the case of compacted soils, the pore size distribution detected by MIP is a good estimate of the real pore size distribution, as reported by Simms and Yanful (2004).

Thermal Conductivity as Related to Packing and Mechanical Properties

The relationship between the initial thermal conductivity, λ_i , and bulk unit weight, γ_b , of compacted mixtures of mine tailings and fly ash is shown in Fig. 12. The initial bulk unit weight is defined as the weight of solids and water per unit volume of specimens immediately after compaction. The initial thermal conductivity increases with increasing initial bulk unit weight with a linear correlation ($R^2 = 0.86$). Similar linear relation between the thermal conductivity and bulk density is found for compacted natural soils (Ekwue et al. 2006; Hotz and Ge 2010). Meanwhile, a linear correspondence exists between the final thermal conductivity, λ_f (i.e., the thermal conductivity measured at 120 hours of curing period) and cumulative pore volume, V_c , by the MIP test, as seen in Fig. 13. The final thermal conductivity is inversely proportional to the cumulative pore volume per unit weight ($R^2 = 0.87$). From such correlations, one may deduce that the thermal conductivity of mine tailings and fly ash mixtures is strongly dependent on the packing properties represented by the initial bulk unit weight and the cumulative pore volume after curing. Hence, these parameters play predominant roles in the heat transfer of wet and dry geomaterials and are key parameters for understanding the microfabrics of geomaterials.

Since the changes of thermal conductivity and strength result from the physicochemical processes of compacted specimens of mine tailings and fly ash mixtures, the relationship between these two properties is considered. Figure 14 illustrates the unconfined compressive strength, q_u , versus the thermal conductivity, λ , for all specimens, which is obtained by combining the relations depicted in Figs. 5 and 7. A positive linear trend between compressive strength and thermal conductivity can be observed: as the curing time increases, compressive strength increases and thermal conductivity decreases; however, the rate of compressive strength gain per the reduction of thermal conductivity decreases with time.

Summary and Conclusions

The thermal conductivity, compressive strength, elastic modulus and temperature changes of compacted specimens of mine tailings and fly ash mixtures during the curing period were investigated as functions of the fly ash ratio, molding water content and compaction energy of the specimens. The pore size distribution and microfabrics of the fly ash treated mine tailings were also examined. The thermal conductivity of the compacted mine tailings and fly ash mixtures was analyzed to relate with their packing and mechanical properties. The significant findings are summarized as follows:

- (1) The addition of fly ash to mine tailings leads to a decrease in the initial thermal conductivity of the specimens. The highest value of the initial thermal conductivity is obtained at the specimen compacted under the optimum water content. The higher compaction energy causes increases in the initial thermal conductivity of the specimens. As the curing time increases, the difference in the initial thermal conductivities decreases.
- (2) For all specimens cured in a temperature-controlled environment, a similar trend of internal temperature variations over time is observed: the temperature decreases at the early stage of the curing period and then increases until it reaches the environmental temperature. The higher fly ash content in specimens induces higher initial temperature of the specimens.
- (3) The unconfined compressive strength of the specimens increases with increasing curing time, though most of the strength gain is attained within the first 24 hours of curing. The increase in the fly ash ratio leads to the increase in the compressive strength of the specimens, indicating that the fly ash is effective in improving the strength of mine tailings by causing cementation. An increase in the molding water content results in a

decrease in the compressive strength of the specimens under the same compaction energy, while a higher compressive strength is achieved at higher compaction energy. In general, the change characteristic of the elastic modulus of the specimens is similar to that of the corresponding unconfined compressive strength.

- (4) A double porosity fabric represented by macropores and micropores is identified in the specimens of mine tailings and fly ash mixtures. As the fly ash ratio increases, both the unit pore volume and mean pore size decreases owing to denser packing. The specimen with the fly ash ratio of 60% displays a monomodal pore size distribution, representing the highest packing density. The mean pore size of the specimen compacted at the dry side of optimum water content is larger than those compacted at the optimum and the wet of optimum, which is mostly attributed to the redistribution of macropores. Increasing compaction energy leads to a substantial reduction in both the macropores and micropores but the bimodal fabric remains unchanged. The surface fabrics of the specimens were investigated using SEM observation, which correlated well with the corresponding pore size distribution indicated by the MIP test.
- (5) Linear relationships are observed between the initial thermal conductivity and bulk unit weight as well as between the final thermal conductivity and cumulative pore volume per unit weight for all specimens tested. The relationship between the thermal conductivity and compressive strength in mine tailings and fly ash mixtures are also established.

The findings presented in this study will be beneficial for understanding the short-term development of thermal and mechanical behaviors of mine tailings treated with fly ash.

Acknowledgements

The authors acknowledge support in this research from the National Science and Engineering Research Council of Canada (NSERC), the University of Western Ontario, Goldcrop Musselwhite Mine and Ontario Power Generation-Atikokan Generating Station.

References

- Aligizaki, K.K. 2006. Pore structure of cement-based materials: testing, interpretation and requirement. Taylor and Francis, London and New York.
- Al-Rawas, A.A. 2002. Microfabric and mineralogical studies on the stabilization of an expensive soil using cement by-pass dust and some types of slags. *Canadian Geotechnical Journal*, **39**(5): 1150-1167.
- ASTM. 2004. Standard practice for characterizing fly ash for use in soil stabilization. ASTM standard D5239-04. American Society for Testing and Materials, West Conshohocken, Pa.
- ASTM. 2007. Standard test methods for laboratory compaction characteristics of soil using standard effort [12,400 ft-lb/ft³ (600 kN-m/m³)]. ASTM standard D698-07. American Society for Testing and Materials, West Conshohocken, Pa.
- ASTM. 2008a. Standard specification for coal fly ash and raw for calcined natural pozzolan for use in concrete. ASTM standard C618-08a. American Society for Testing and Materials, West Conshohocken, Pa.
- ASTM. 2008b. Standard test method for determination of thermal conductivity of soil and soft rock by thermal needle probe procedure. ASTM standard D5334-08. American Society for Testing and Materials, West Conshohocken, Pa.

- ASTM. 2009a. Standard test methods for laboratory compaction characteristics of soil using modified effort [56,000 ft-lb/ft³ (2700 kN-m/m³)]. ASTM standard D1557-09. American Society for Testing and Materials, West Conshohocken, Pa.
- ASTM. 2009b. Standard test methods for unconfined compressive strength of compacted soil-lime mixtures. ASTM standard D5102-09. American Society for Testing and Materials, West Conshohocken, Pa.
- Bussiere, B. 2007. Colloquium 2004: hydrogeotechnical properties of hard rock tailings from metal mines and emerging geoenvironmental disposal approaches. *Canadian Geotechnical Journal*, **44**(9): 1019-1052.
- Cetin, B., Aydilek, A.H., and Guney, Y. 2010. Stabilization of recycled base materials with high carbon fly ash. *Resources, Conservation and Recycling*, **54**(11): 878-892.
- Choquette, M., Berube, M., and Locat, J. 1987. Mineralogical and microtextural changes associated with lime stabilization of marine clays from Eastern Canada. *Applied Clay Science*, **2**(3): 215-232.
- Cote, J., and Konrad, J. 2009. Assessment of structure effects on the thermal conductivity of two-phase porous geomaterials. *International Journal of Heat and Mass Transfer*, **52**(3-4): 796-804.
- Cuisinier, O., Auriol, J., Le Borgne, T., and Deneele, D. 2011. Microstructure and hydraulic conductivity of a compacted lime-treated soil. *Engineering Geology*, **123**(3): 187-193.
- Degirmenci, N., Okucu, A., and Turabi, A. 2007. Application of phosphogypsum in soil stabilization. *Building and Environment*, **42**(9): 3393-3398.

- Daniel, D.E., and Benson, C.H. 1990. Water content-density criteria for compacted soil liners. *Journal of Geotechnical Engineering*, **116**(12): 1811-1830.
- Daniel, D.E., and Wu, Y. 1993. Compacted clay liners and covers for arid sites. *Journal of Geotechnical Engineering*, **119**(2): 223-237.
- Delage, P. 2010. A microstructure approach to the sensitivity and compressibility of some Eastern Canada sensitive clays. *Geotechnique*, **60**(5): 353-368.
- Delage, P., Audiguier, M., Cui, Y., and Howat, M.D. 1996. Microstructure of a compacted silt. *Canadian Geotechnical Journal*, **33**(1): 150-158.
- Edil, T.B., Acosta, H.A., and Benson, C.H. 2006. Stabilizing soft fine-grained soils with fly ash, *Journal of Materials in Civil Engineering*, **18**(2): 283-294.
- Ekwue, E.I., Stone, R.J., and Bhagwat, D. 2006. Thermal conductivity of some compacted Trinidadian soils as affected by peat content. *Biosystems Engineering*, **94**(3): 461-469.
- Fall, M., Celestin, J.C., and Han, F.S. 2009. Suitability of bentonite-paste tailings mixtures as engineering barrier material for mine waste containment facilities. *Minerals Engineering*, **22**(9-10): 840-848.
- Ghosh, A., and Subbarao, C. 2007. Strength characteristics of class F fly ash modified with lime and gypsum. *Journal of Geotechnical and Geoenvironmental Engineering*, **133**(7): 757-766.
- Guney, Y., Aydilek, A.H., and Demirkan, M.M. 2006. Geoenvironmental behavior of foundry sand amended mixture for highway subbases. *Waste Management* **26**(9): 932-945.

- Helinski, M., Fahey, M., and Fourie, A. 2011. Behavior of cemented paste backfill in two mine stopes: measurements and modeling. *Journal of Geotechnical and Geoenvironmental Engineering*, **137**(2): 171-182.
- Horpibulsuk, S., Rachan, R., and Raksachon, Y. 2009. Role of fly ash on strength and microstructure development in blended cement stabilized silty clay. *Soils and Foundations*, **49**(1): 85-89.
- Hotz, R.D., and Ge, L. 2010. Investigation of the thermal conductivity of compacted silts and its correlation to the elastic modulus. *Journal of Materials in Civil Engineering*, **22**(4): 408-412.
- Indraratna, B., Nutalaya, P., and Kuganenthira, N. 1991. Stabilization of a dispersive soil by blending with fly ash. *Quarterly Journal of Engineering Geology*, **24**(3): 275-290.
- Juang, C.H., and Holtz, R.D. 1986. Fabric, pore size distribution, and permeability of sandy soils. *Journal of Geotechnical Engineering*, **112**(9): 855-868.
- Kolay, P.K., and Singh, D.N. 2002. Application of coal ash in fluidized thermal beds. *Journal of Materials in Civil Engineering*, **14**(5): 441-444.
- Kolias, S., Kasselouri-Rigopoulou, V., and Karahalios, A. 2005. Stabilization of clayey soils with high calcium fly ash and cement. *Cement and Concrete Composites*, **27**(2): 301-313.
- Lade, P.V., Liggió, C.D., and Yamamuro, J.A. 1998. Effects of non-plastic fines on minimum and maximum void ratios of sand. *Geotechnical Testing Journal*, **21**(4): 1173-1188.
- Nalbantoglu, Z., and Tuncer, E.R. 2001. Compressibility and hydraulic conductivity of a chemically treated expansive clay. *Canadian Geotechnical Journal*, **38**(1): 154-160.

- Osinubi, K.J. 1998. Influence of compactive efforts and compaction delays on lime-treated soil. *Journal of Transportation Engineering*, **124**(2): 149-155.
- Ozyildirim, C., and Carino, N.J. 2006. Concrete strength testing. *In* Significance of tests and properties of concrete and concrete-making materials. Edited by J.E. Lamond and J.H. Pielert. ASTM STP 169D. American Society for Testing and Materials, West Conohocken, Pa. pp. 125-140.
- Peethamparan, S., Olek, J., and Lovell, J. 2008. Influence of chemical and physical characteristics of cement kiln dusts (CKDs) on their hydration behavior and potential suitability for soil stabilization. *Cement and Concrete Research*, **38**(6): 803-815.
- Penumadu, D., and Dean, J. 2000. Compressibility effect in evaluating the pore-size distribution of kaolin clay using mercury intrusion porosity. *Canadian Geotechnical Journal*, **37**(2): 393-405.
- Phanikumar, B.R., and Sharma, R.S. 2007. Volume change behavior of fly-ash-stabilized clays. *Journal of Materials in Civil Engineering*, **19**(1): 67-74.
- Pilito, C.P., and Martin, II J.R. 2001. Effects of nonplastic fines on the liquefaction resistance of sands. *Journal of Geotechnical and Geoenvironmental Engineering*, **127**(5): 408-415.
- Qian, G., Haung, T., and Bai, S. 2011. Use of cement-stabilized granite mill tailings as pavement subbase. *Journal of Materials in Civil Engineering*, **23**(11): 1575-1578.
- Sawangsurriya, A., Edil, T.B., and Bosscher, P.J. 2008. Modulus-suction-moisture relationship for compacted soil. *Canadian Geotechnical Journal*, **45**(7): 973-983.

- Simms, P.H., and Yanful, E.K. 2001. Measurement and estimation of pore shrinkage and pore distribution in a clayey till during soil-water characteristics curve tests. *Canadian Geotechnical Journal*, **38**(4): 741-754.
- Simms, P.H., and Yanful, E.K. 2004. A discussion of the application of mercury intrusion porosimetry for the investigation of soils, including an evaluation of its use to estimate volume change in compacted clayey soils. *Geotechnique*, **54**(6): 421-426.
- Solanki, P., Khoury, N., and Zaman, M.M. 2009. Engineering properties and moistures susceptibility of silty clay stabilized with lime, class C fly ash, and cement kiln dust. *Journal of Materials in Civil Engineering*, **21**(12): 749-757.
- Tarantino, A., and De Col, E. 2008. Compaction behaviour of clay. *Geotechnique*, **58**(3): 199-213.
- Tastan, E.O., Edil, T.B., Benson, C.H., and Aydilek, A.H. 2011. Stabilization of organic soils with fly ash. *Journal of Geotechnical and Geoenvironmental Engineering*, **137**(9): 819-833.
- Thevanayagam, S., Shenthana, T., Mohan, S., and Liang, J. 2002. Undrained fragility of clean sands, silty sands and sandy silts. *Journal of Geotechnical and Geoenvironmental Engineering*, **128**(10): 849-859.
- Wang, H.L., Shang, J.Q., Kovac, V., and Ho, K.S. 2006. Utilization of Atikokan coal fly ash in acid rock drainage control from Musselwhite mine tailings. *Canadian Geotechnical Journal*, **43**(3), 229-243.
- Washburn, E.W. 1921. Note on a method of determining the distribution of pore sizes in a porous material. *Proceedings of the National Academy of Science*, **7**(4), 115-116.

Yang, S.R, Haung, W.H., and Tai, Y.T. 2005. Variation of resilient modulus with soil suction for compacted subgrade soils. *Transportation Research Record*, 1913, 99-106.

Yeheyis, M.B., Shang, J.Q., and Yanful, E.K. 2009. Long-term evaluation of coal fly ash and mine tailings co-placement: a site-specific study. *Journal of Environmental Engineering*, **91**(1): 237-244.

Yilmaz, Y. 2009. A study on the limit void ratio characteristics of medium to fine mixed graded sands. *Engineering Geology*, **104**(3-4): 290-294.

List of Symbols

C_c	coefficient of curvature
C_u	coefficient of uniformity
D_{10}	effective size of particles (μm)
D_{50}	median size of particles (μm)
d	specimen diameter (m)
d_p	pore diameter (μm)
E	elastic modulus (MPa)
G_s	specific gravity
h	specimen height (m)
P	mercury intrusion pressure (MPa)
P_{FA}	percentage of fly ash weight in total mixture weight (%)
q_u	unconfined compressive strength (MPa)
R_{FA}	fly ash ratio (%)
T	temperature ($^{\circ}\text{C}$)
T_s	surface tension (N/m)

t	curing time (hours)
V_c	cumulative pore volume per unit weight (mL/g)
V_d	derivative of the cumulative pore volume with respect to pore size (mL/g/ μm)
W_{FA}	weight of fly ash (g)
W_{MT}	weight of mine tailings (g)
w_{opt}	optimum water content (%)
w	molding water content (%)
γ_b	bulk unit weight (kN/m ³)
γ_d	dry unit weight (kN/m ³)
$\gamma_{d\max}$	maximum dry unit weight (kN/m ³)
θ	contact angle (degrees)
λ	thermal conductivity (W/mK)
λ_f	final thermal conductivity (W/mK)
λ_i	initial thermal conductivity (W/mK)

Table 1 Physical properties of test materials.

Properties	Mine tailings	Fly ash
Specific gravity, G_s	3.37	2.54
Optimum water content, w_{opt} (%) †	12.6	11.9
Maximum dry unit weight, $\gamma_{d\max}$ (kN/m ³) †	20.4	16.6
Effective size, D_{10} (μm)	2.8	0.8
Median size, D_{50} (μm)	25.6	15.2
Coefficient of uniformity, C_u	11.43	25.61
Coefficient of curvature, C_c	1.61	2.61

† ASTM D 698-07 (ASTM 2007)

Table 2 Oxide composition of test materials (adapted from Wang et al. 2006).

Component (%)	Mine tailings	Fly ash
SiO ₂	50.82	37.99
Al ₂ O ₃	8.87	19.92
Fe ₂ O ₃	28.97	6.17
MnO	0.36	0.03
MgO	3.39	3.52
CaO	3.19	15.66
K ₂ O	0.84	0.62
Na ₂ O	0.02	9.30
P ₂ O ₅	0.15	0.69
Cr ₂ O ₃	0.02	0.00
TiO ₂	0.45	0.84
Loss on ignition	0.05	0.68
Total	97.13	95.12

Table 3 Summary of specimens tested.

Specimen ID [†]	Water content, w (%)	Dry unit weight, γ_d (kN/m ³)
FA20 - SP - OWC	12.4	19.5
FA40 - SP - OWC	11.6	19.2
FA60 - SP - OWC	11.0	18.9
FA20 - SP - DWC	10.5	19.2
FA20 - SP - WWC	14.3	19.0
FA20 - HP - OWC	12.4	20.0

Note: FA = fly ash; OWC = optimum water content; DWC = dry water content; WWC = wet water content; SP = standard Proctor energy (590 kJ/m³); HP = high Proctor energy (1,190 kJ/m³); the numbers that follow the FA indicate the percentage by weight of fly ash added to the mine tailings.

[†] Each specimen consists of five samples with identical properties of mine tailings and fly ash mixtures.

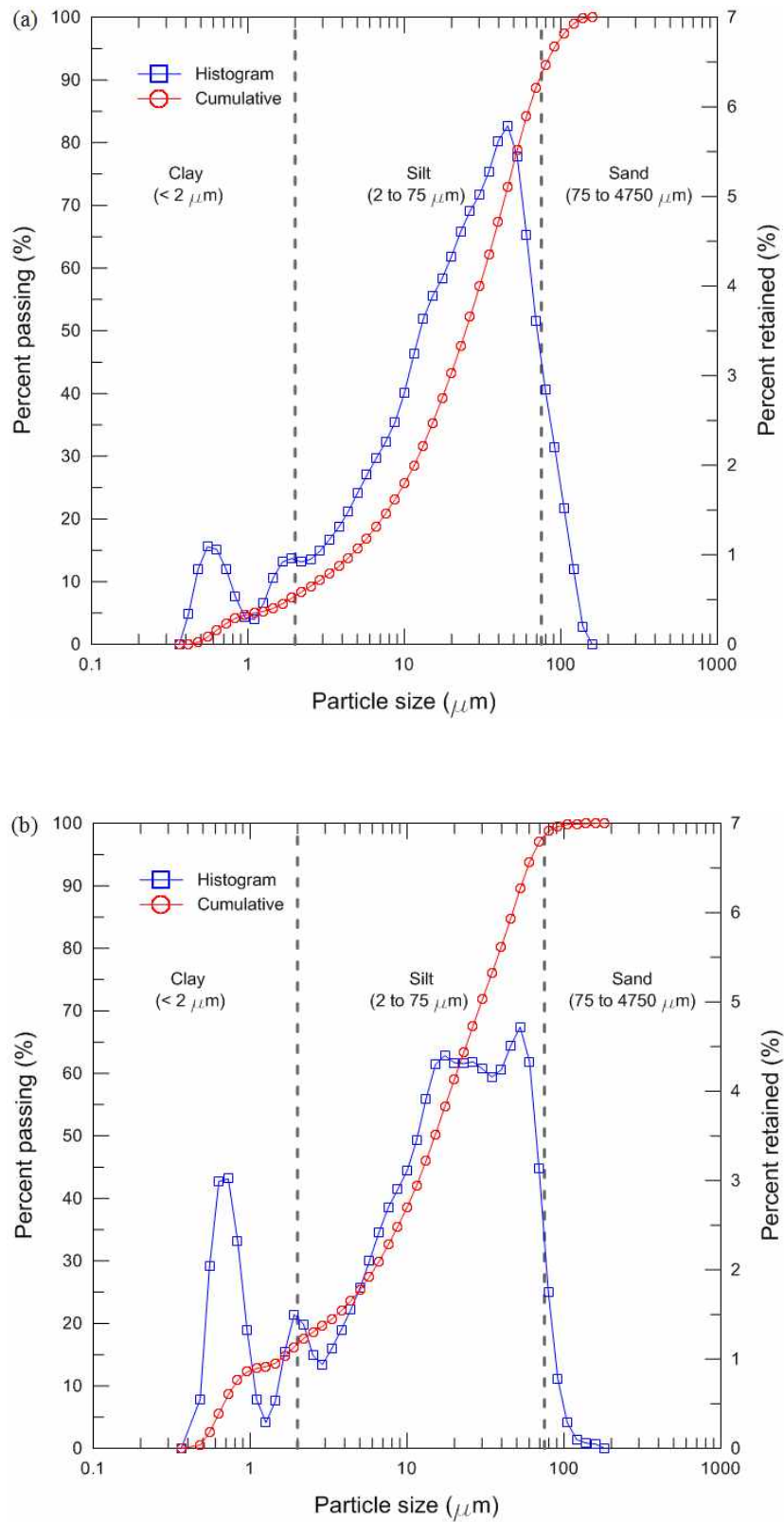


Fig. 1 Particle size distributions of (a) Musselwhite mine tailings and (b) Atikokan fly ash.

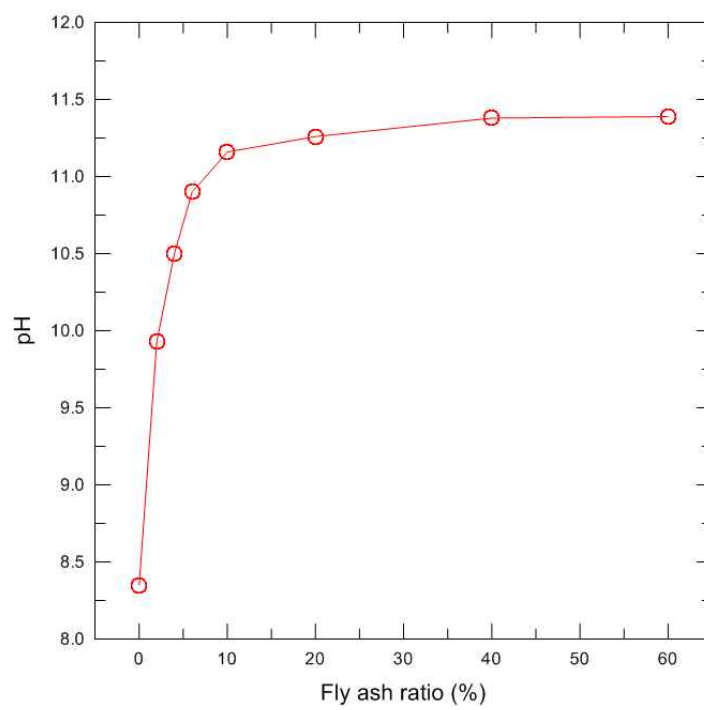


Fig. 2 pH variation of mixtures of mine tailings and fly ash.

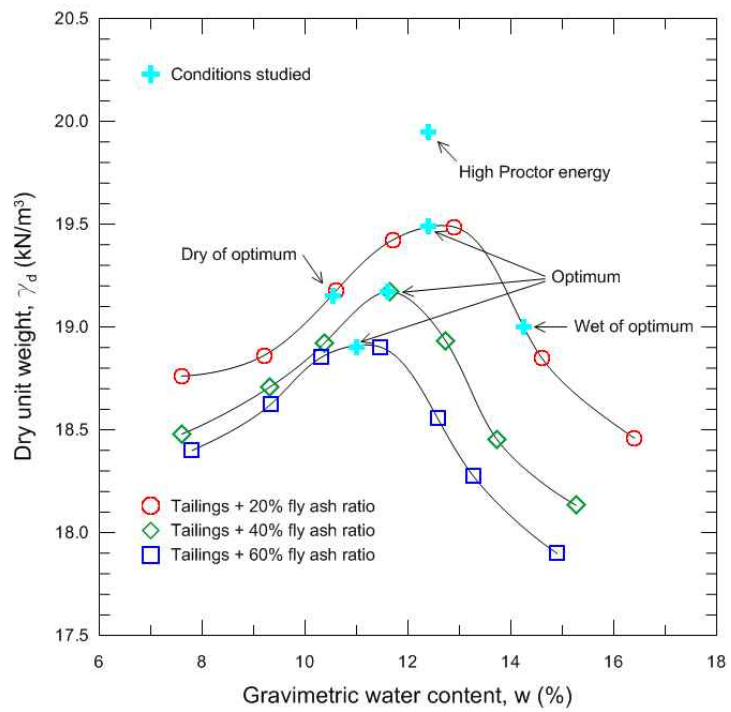


Fig. 3 Compaction curves and conditions studied.

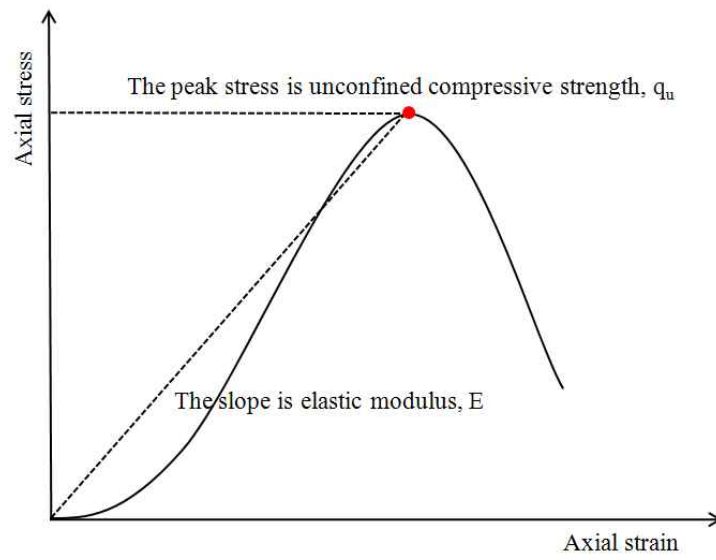


Fig. 4 Typical stress and strain curve of compacted mine tailings and fly ash mixtures.

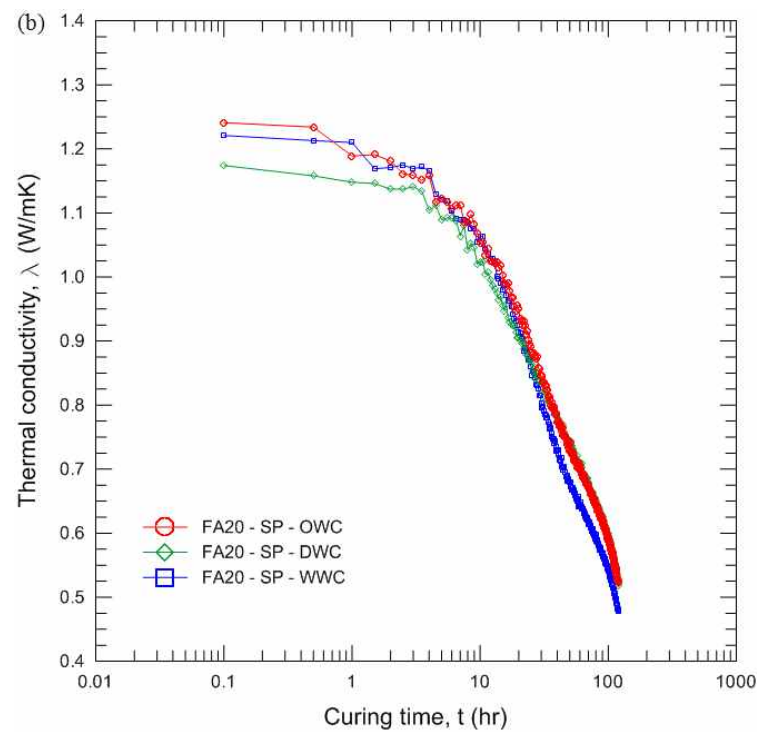
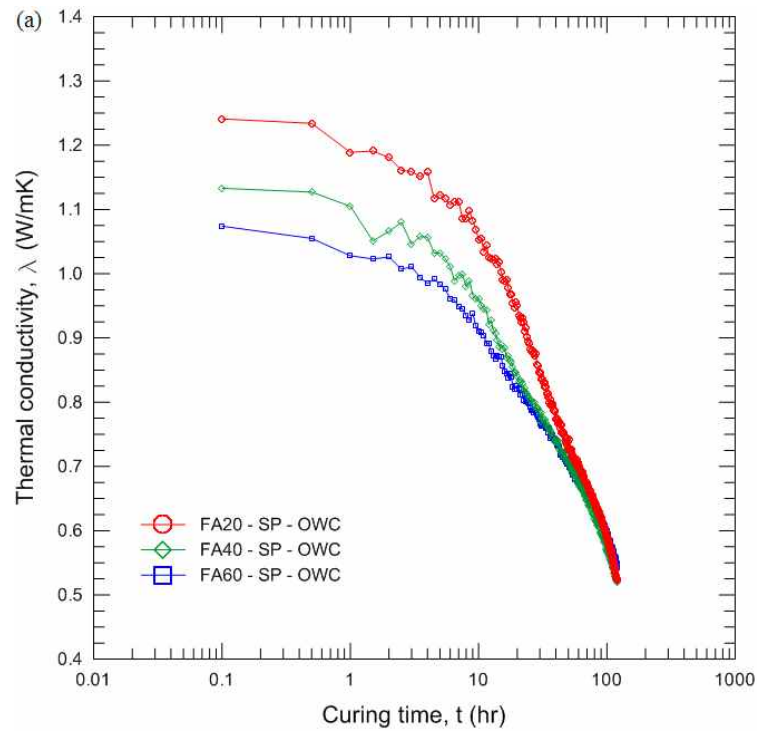


Fig. 5 Variations of thermal conductivity with curing time: effects of (a) fly ash ratio, (b) molding water content, and (c) compaction energy.

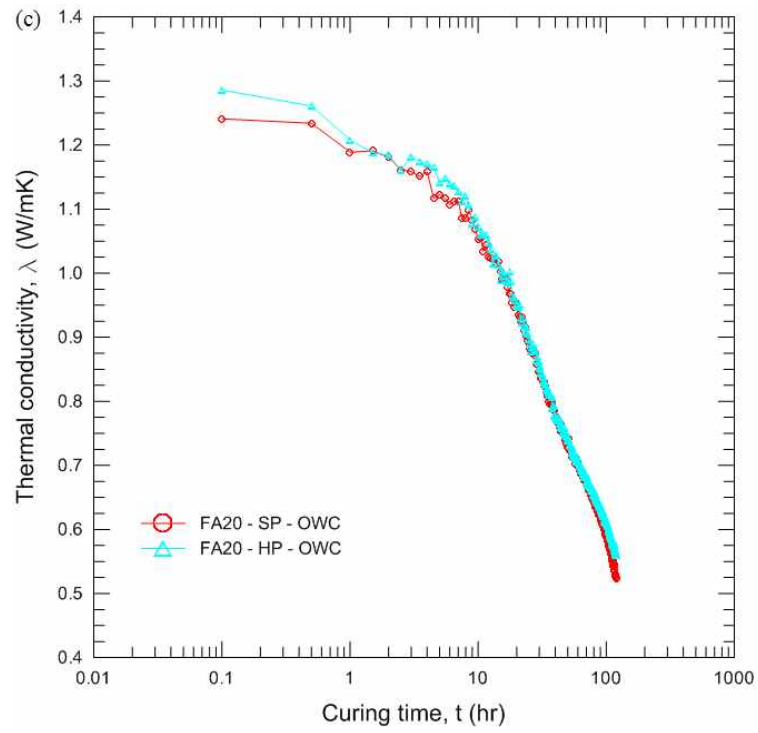


Fig. 5 Variations of thermal conductivity with curing time: effects of (a) fly ash ratio, (b) molding water content, and (c) compaction energy (continued).

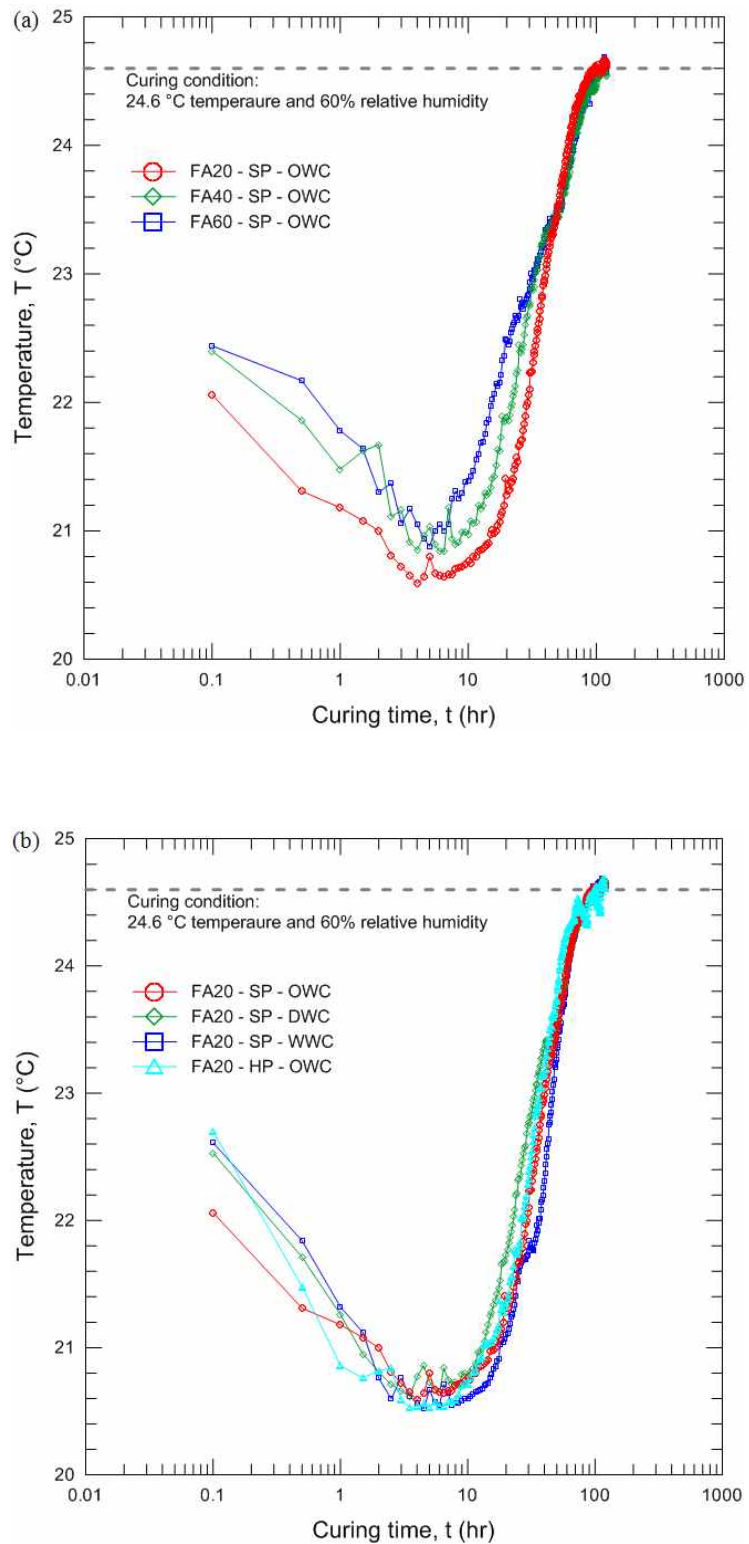


Fig. 6 Variations of temperature with curing time: effects of (a) fly ash ratio and (b) molding water content and compaction energy.

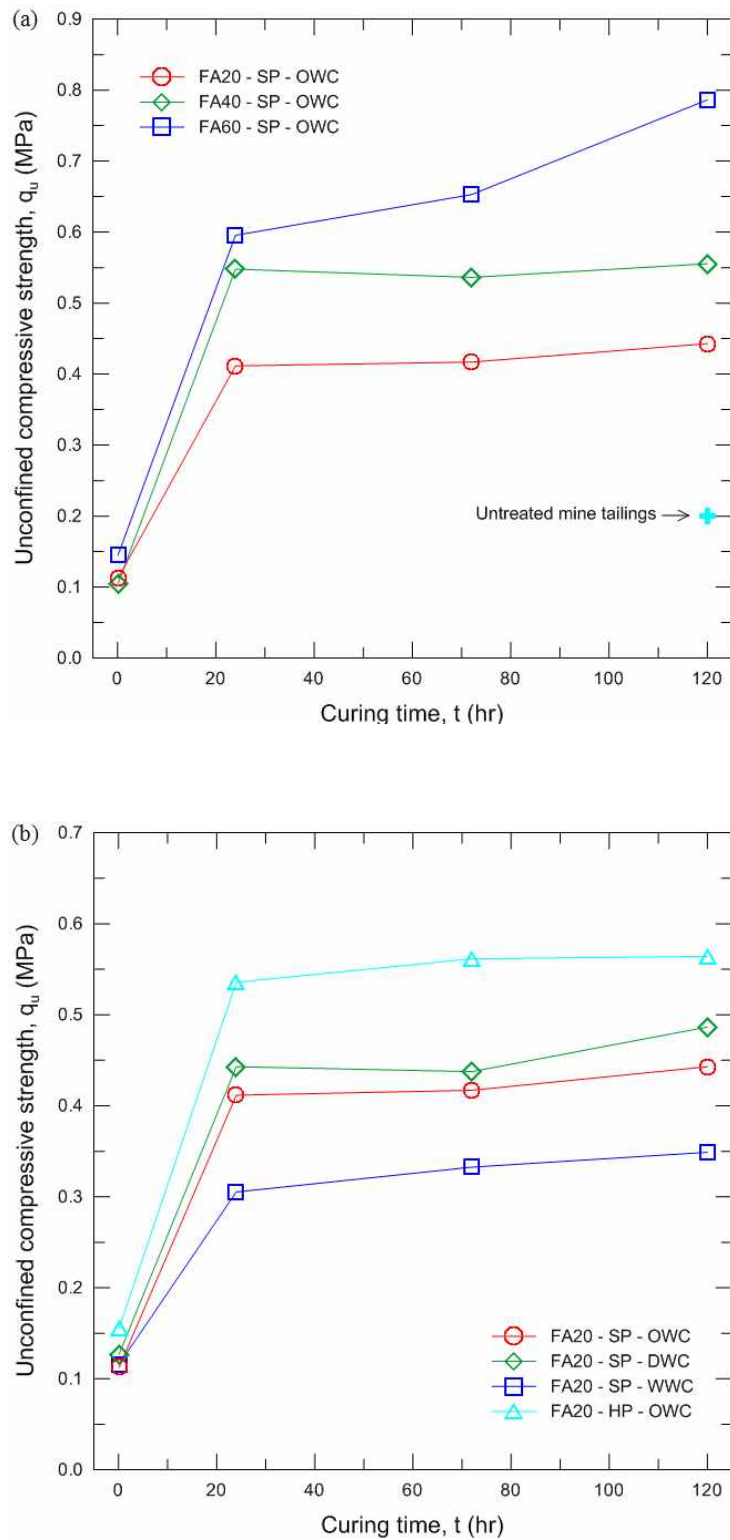


Fig. 7 Variations of unconfined compressive strength with curing time: effects of (a) fly ash ratio and (b) molding water content and compaction energy.

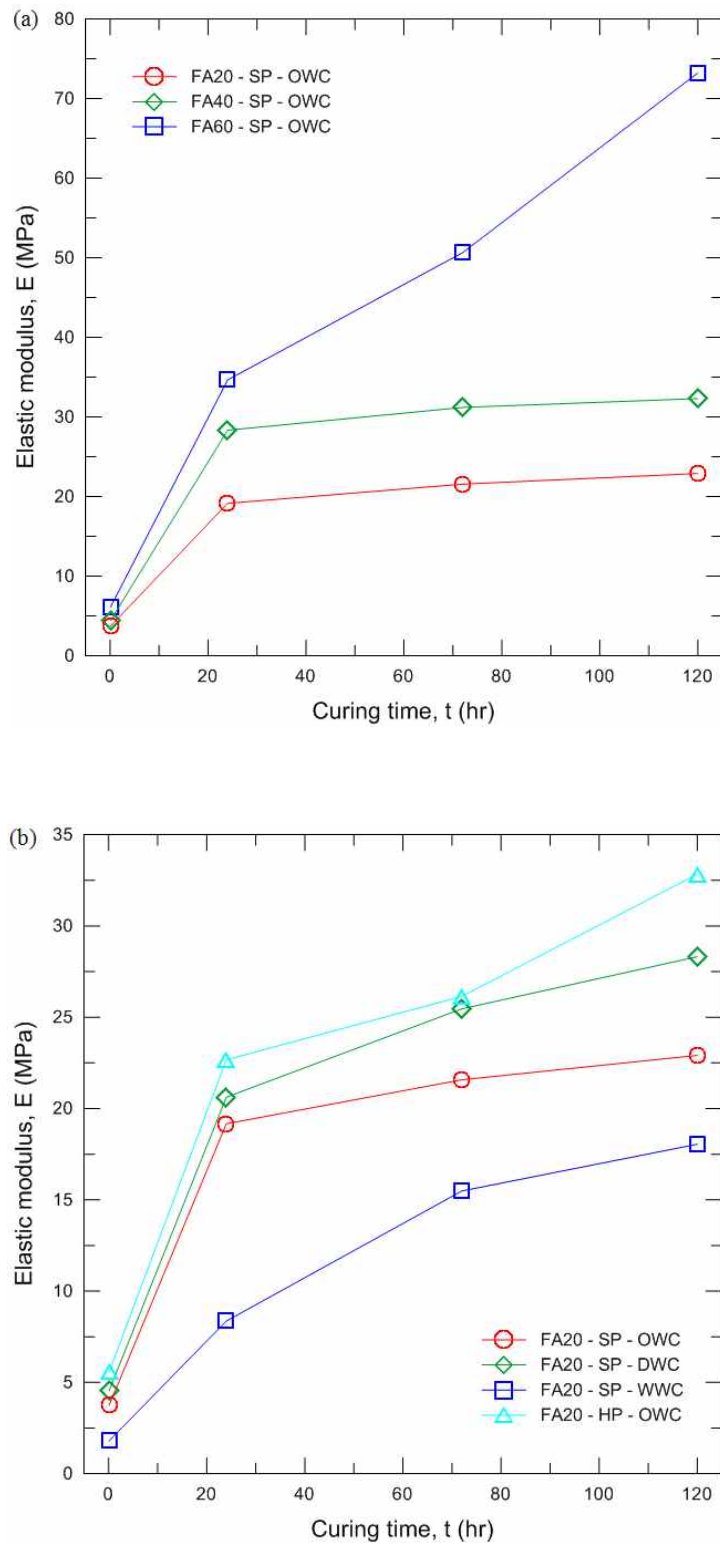


Fig. 8 Variations of elastic modulus with curing time: effects of (a) fly ash ratio and (b) molding water content and compaction energy.

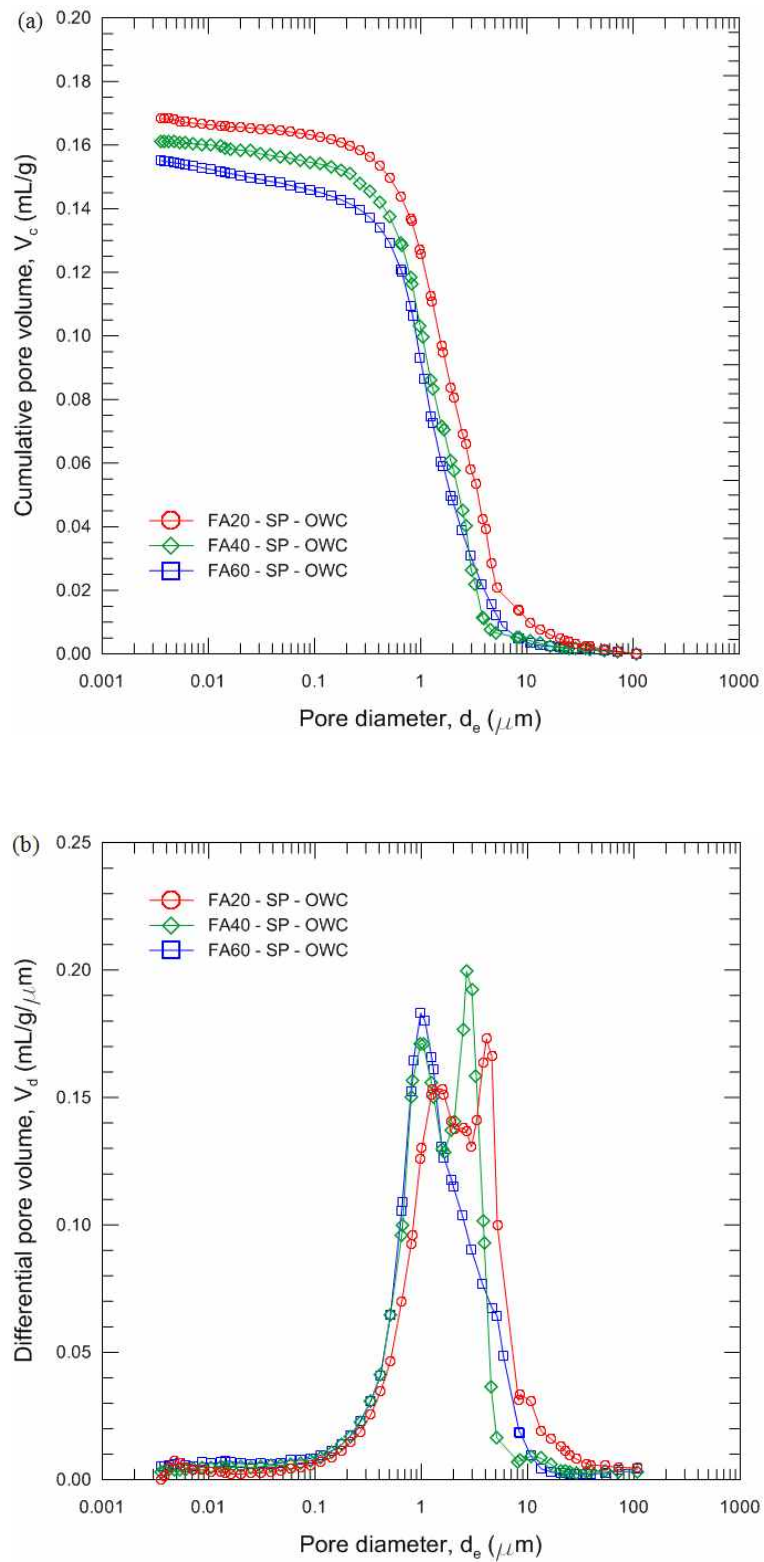


Fig. 9 Mercury intrusion porosimetry results of the 120 hours-cured specimens with different fly ash contents (20, 40 and 60%): (a) cumulative pore volume; (b) differential pore volume.

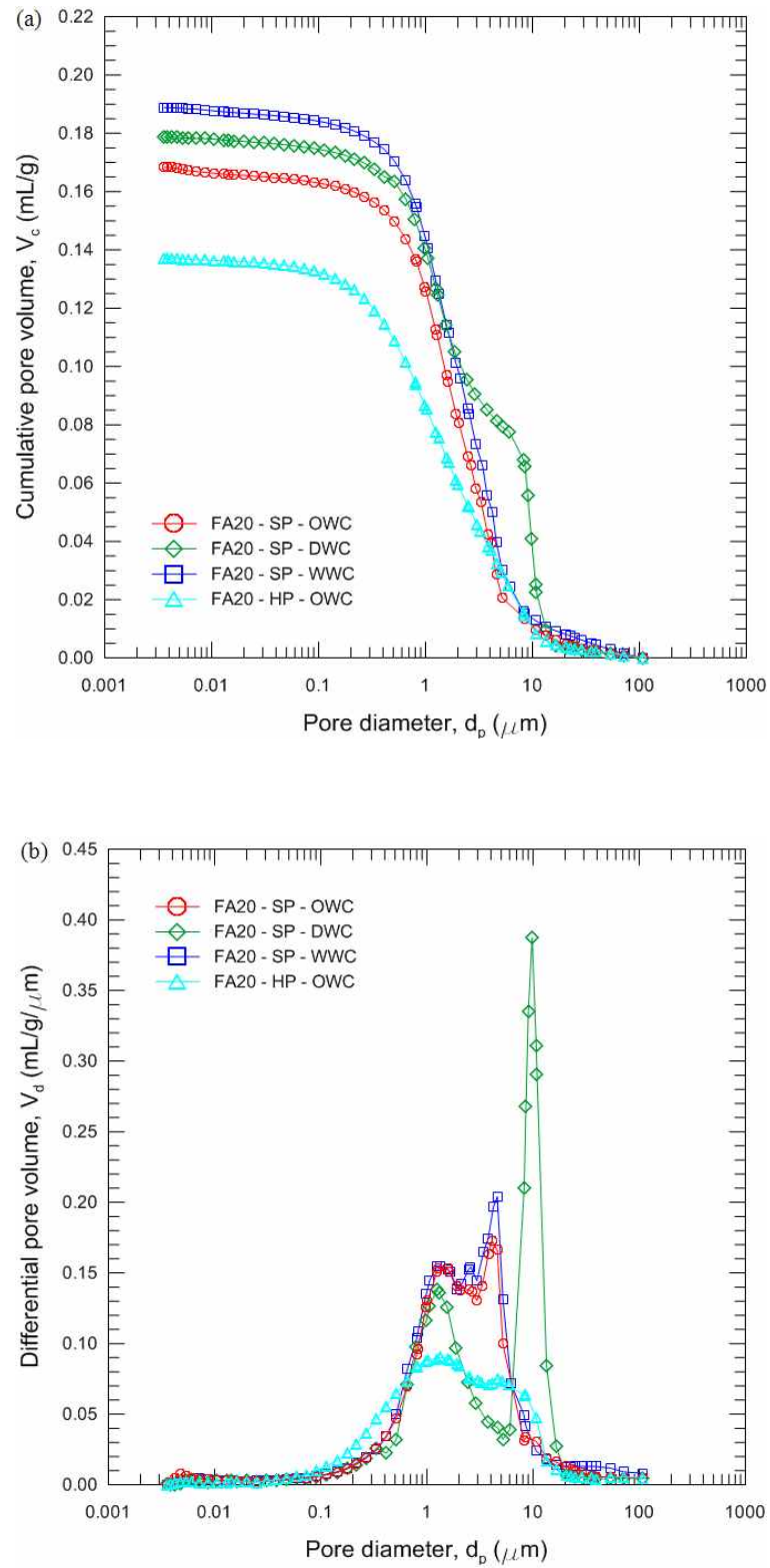


Fig. 10 Mercury intrusion porosimetry results of the 120 hours-cured specimens compacted at different compaction conditions: (a) cumulative pore volume; (b) differential pore volume.

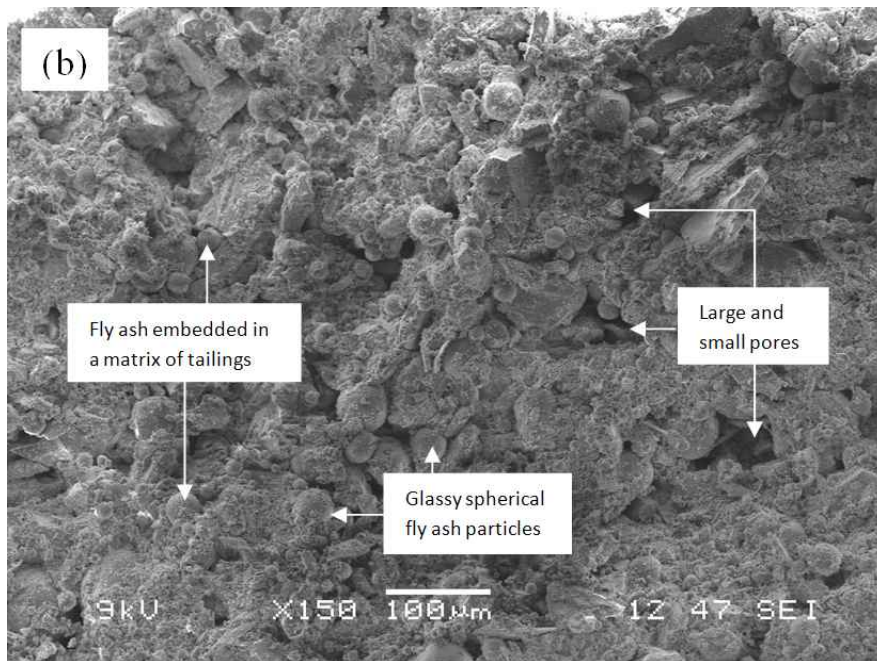
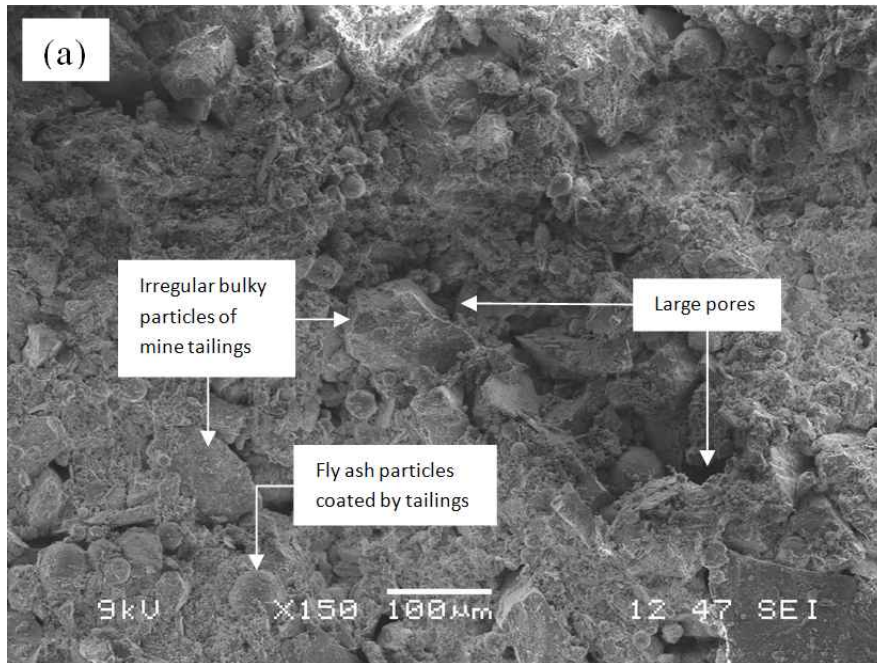


Fig. 11 SEM images of the 120 hours-cured samples with different fly ash contents: (a) FA = 20%; (b) FA = 40%; (c) FA = 60%.

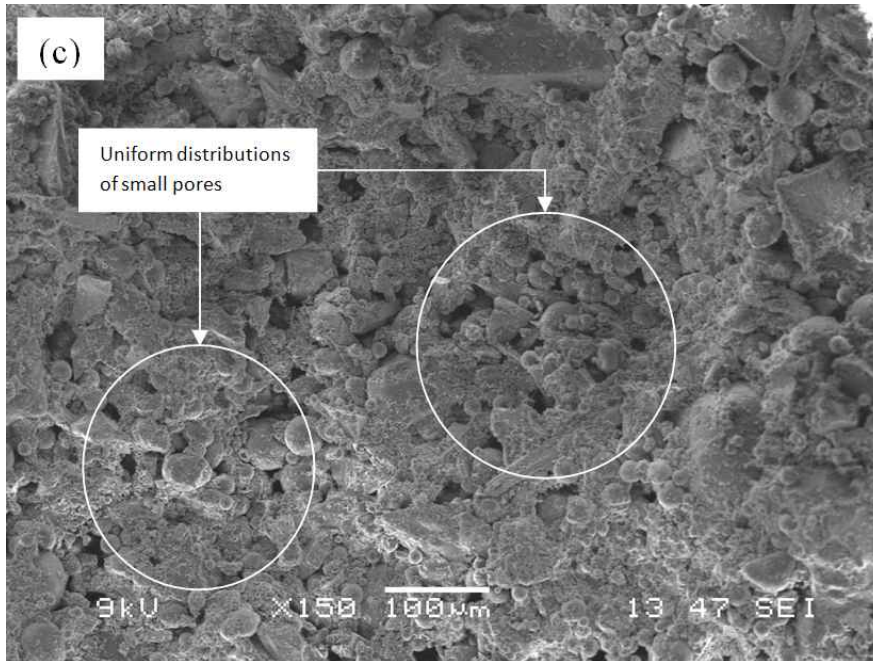


Fig. 11 SEM images of the 120 hours-cured samples with different fly ash contents: (a) FA = 20%; (b) FA = 40%; (c) FA = 60% (continued).

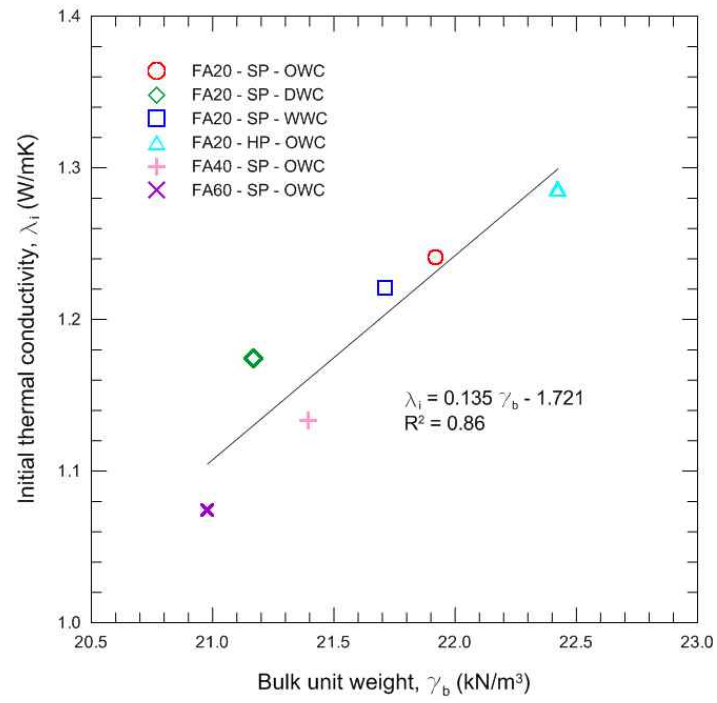


Fig. 12 Relationship between initial thermal conductivity and bulk unit weight.

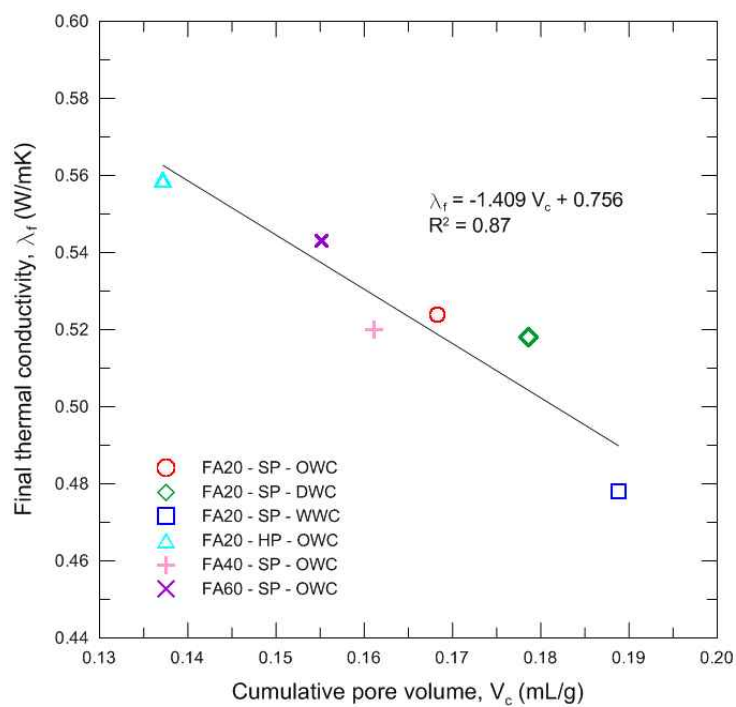


Fig. 13 Relationship between final thermal conductivity and cumulative pore volume.

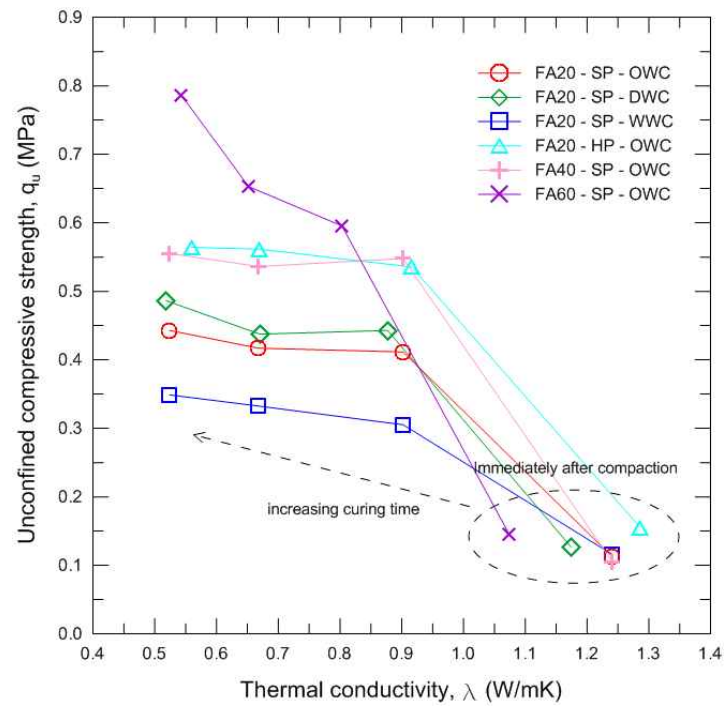


Fig. 14 Relationship between unconfined compressive strength and thermal conductivity.